Kinetic energy recovery and interface hysteresis of bouncing droplets after inelastic head-on collision

Cite as: Phys. Fluids **29**, 103306 (2017); https://doi.org/10.1063/1.5000547
Submitted: 17 August 2017 . Accepted: 03 October 2017 . Published Online: 23 October 2017

Zhenyu Zhang, and Peng Zhang

Kinetic energy recovery and interface hysteresis of bouncing droplets after inelastic head-on collision

Zhenyu Zhang and Peng Zhang[a)]
Department of Mechanical Engineering, The Hong Kong Polytechnic University, Hong Kong 999077, People's Republic of China

(Received 17 August 2017; accepted 3 October 2017; published online 23 October 2017)

Binary collision of unequal-size droplets was investigated numerically by using the front tracking method, with particular emphasis in studying the kinetic energy recovery and the interface hysteresis of bouncing droplets. The numerical results were sufficiently validated against the high-quality experimental data in the literature to verify the quantitative predictivity of the numerical methodology in simulating droplet bouncing. Distinct stages of droplet deformation and viscous dissipation during droplet collision were revealed and explained for their dependence on the Weber number and the size ratio. A linear fitting formula that well correlates the kinetic energy recovery factor of bouncing droplets with various collision parameters was proposed and would be practically useful in modeling inelastic droplet bouncing in Lagrangian spray simulation. As an interesting post-collision characteristic of bouncing droplets, the interface hysteresis was found to favor smaller droplet deformation by decreasing the size ratio or decreasing the Weber number or increasing the Ohnesorge number. *Published by AIP Publishing.* https://doi.org/10.1063/1.5000547

I. INTRODUCTION

Energy conversion efficiency and exhaust emissions of many combustion energy conversion devices greatly rely on dispersed gas-liquid two-phase flows, particularly on the accompanying phenomena of droplet collision and breakup. A prominent example is the dense spray of liquid fuel in the combustion chamber of a diesel, gas-turbine, or rocket engine, where the large number density of droplets together with the non-uniform gas flow affect frequent droplet collisions. The collision outcomes, such as coalescence, bouncing, and separation, would change the number density and the distributions of droplet size and droplet velocity, which in turn influence the subsequent spray and combustion characteristics.[1]

As a fundamental multiphase flow problem, binary droplet collision has been studied since 1960s. Early experimental studies[2–4] on water droplet collision in an atmospheric environment were motivated by understanding the formation of rain drops. The observed collision outcomes, such as stretching separation and coalescence, were found to depend on two nondimensional parameters: the Weber number, We, measures the relative importance of the droplet inertia compared with the surface tension, and the impact parameter, B, measures the deviation of the trajectory of droplets from that of head-on collision, with $B = 0$ denoting head-on collision and $B = 1$ denoting grazing collision. Other influence parameters include the size ratio, Δ, which is usually defined as the radius ratio of the larger droplet to the smaller one, and the Ohnesorge number, Oh, which compares the viscous forces with inertial and surface tension forces.

In their study of the head-on collision of equal-size alkane droplets, Jiang *et al.*[5] and Qian and Law[6] first observed droplet bouncing, which is absent in the head-on collision of water droplets. Qian and Law[6] gave a unified description of droplet collision outcomes by presenting five distinct collision regimes in a *We-B* nomograph, namely (Regime I) coalescence after minor deformation, (Regime II) bouncing, (Regime III) coalescence after substantial deformation, (Regime IV) coalescence followed by separation for near head-on collision (also known as reflective separation), and (Regime V) coalescence followed by separation for off-center collision (also known as stretching separation). Droplet bouncing was also observed by Estrade *et al.*[7] for equal-size ethanol droplets and by Tang *et al.*[8] for unequal-size alkane droplets.

Most studies on binary droplet collision were concerned with the transition between different collision regimes,[3–14] the viscous dissipation during collision,[5,6,8,15] the energy conversion,[16,17] the inter-mixing within coalesced droplet,[17–20] and the non-Newtonian effects.[21–23] Much understanding has been obtained on droplet coalescence (Regimes I and III) and separation (Regimes IV and V), but not on droplet bouncing (Regime II). Although droplet bouncing does not change the size distribution of droplets, it can change the spatial distribution of droplets and therefore the subsequent mixture formation and combustion.[24] This is because droplet collision is inelastic,[5,6,10] and the post-collision velocities of bouncing droplets are substantially smaller than the prior-collision impact velocities because of the viscous dissipation of the droplet internal flow induced by droplet deformation.

It is recognized that droplet bouncing becomes particularly prominent under elevated ambient pressures. Qian and Law[6] experimentally observed that bouncing is significantly promoted by increasing the ambient pressure from 0.6 atm

a)Author to whom correspondence should be addressed: pengzhang.zhang@polyu.edu.hk.

to 12 atm. The theoretical analysis of Zhang and Law[15] demonstrates that the gas film between two colliding droplets is harder to be drained out under elevated pressures to trigger droplet coalescence. By implementing Zhang and Law's[15] theory into a volume-of-fluid (VOF) code, Li[25] successfully simulated droplet collision under different ambient pressures without numerical artifacts. Recently, the molecular dynamics simulation of Zhang *et al.*[26] also confirms that colliding droplets tend to bounce off with increasing the ambient pressure. To demonstrate the important role of droplet bouncing in Lagrangian spray simulation, Zhang *et al.*[27] numerically investigated the impinging sprays under high ambient pressures and found that the propensity of droplet bouncing with increasing pressure must be taken into account to explain the experimental observations.

Droplet collision modeling is an indispensable component in the Lagrangian simulation of sprays. Worthy progress has been made in predicting the droplet collision probability[28–31] and in parameterizing the complex collision outcomes.[4,7,15,32–37] Determining the post-collision characteristics of bouncing droplets has however not been sufficiently studied. By accounting for the viscous dissipation during droplet bouncing, O'Rourke[32] defined a kinetic energy recovery factor, $1-f_E$, by

$$1-f_E=\frac{KE'}{KE}, \tag{1}$$

where KE and KE' are the total droplet kinetic energy before and after bouncing, respectively, and they are calculated in the center of mass frame of reference. f_E is also known as the energy dissipation fraction of the collision. O'Rourke proposed an empirical model as

$$1-f_E=\left(\frac{B-B_{cr}}{1-B_{cr}}\right)^2, B_{cr}=\sqrt{min(1.0,[2.4f(\Delta)/We])},$$
$$f(\Delta)=\Delta^{-3}-2.4\Delta^{-2}+2.7\Delta^{-1}, \tag{2}$$

where B_{cr} is the transition impact parameter from coalescence ($B\le B_{cr}$) to grazing ($B>B_{cr}$). This model was adopted by the widely used computer program KIVA[38] and subsequently employed by a number of numerical simulations on spray combustion, which have been summarized in Refs. 34–37. Jiang *et al.*[5] and Qian and Law[6] experimentally and theoretically analyzed the energy dissipation during equal-size droplet collision and found that f_E can be as large as 50%, which was subsequently adopted by Zhang *et al.*[27] as a rough estimation in their simulation of impinging sprays. The dependence of f_E on various collision parameters, such as We, Δ, and Oh, has however not been accurately quantified up to date.

Compared with equal-size droplet collision, collision between two unequal-size droplets is more relevant to practical situations. Ashgriz and Poo[4] experimentally found that separation becomes more difficult for water droplets as the size ratio increases. This observation was subsequently confirmed by Testik[11] and Rabe *et al.*[12] for water droplets and by Estrade *et al.*[7] for ethyl alcohol droplets. A recent experimental and theoretical study of Tang *et al.*[8] shows that the increased size ratio has a slight influence on the transition Weber number from bouncing (Regime II) to coalescence (Regime III) although it has a significant influence on that from coalescence (Regime III) to separation (Regime IV). Nevertheless, bouncing of unequal-size droplets has not been gained enough attentions so that the evolution of the droplet interface, the conversion among various forms of energy, and the post-collision characteristics remain inadequately understood up to now.

The present study aims to numerically investigate the bouncing of unequal-size droplets, with particular interest in quantifying the kinetic energy recovery (or equivalently the energy dissipation fraction) during collision. A practical correlation for predicting the post-collision kinetic energy of droplets was proposed and validated against the present numerical results. The interface hysteresis of bouncing droplets was also investigated to understand the interesting post-collision phenomenon, where the colliding interfaces of bouncing droplets tend to approach each other while the centers of mass of the droplets are departing from one another. In the following text, we shall first expatriate the numerical methodology in Sec. II, followed by the results and discussion in Sec. III.

II. NUMERICAL METHODOLOGY

A. Formulation and numerical specifications

The present study adopts the Front Tracking method (referred to as FTM hereinafter) developed by Tryggavason and his colleagues.[39,40] The FTM traces phase interfaces in a Lagrangian framework, while it solves the multiphase flow in a unified domain and in a grid of Eulerian coordinates. The FTM has been widely used in simulating many multiphase flow problems[16,17,40,41] and has demonstrated its prominent advantages in accurately capturing moving interfaces with relatively coarse meshes and therefore with remarkably reduced computational load.

The FTM adopted in the present study has been discussed in detail in the literature[28,40] and implemented in an axisymmetric flow solver that was used by Nobari *et al.*,[41] Qian and Law,[6] Pan *et al.*,[16] and one of the present authors[17] for studying binary droplet collision. As a brief summary of the formulation of the present FTM, a conservative, second-order centered difference scheme for the spatial variables and an explicit first-order time integration method were used to solve the governing equations for incompressible flows for both liquid and gas phases, given by

$$\nabla\cdot\boldsymbol{V}=0, \tag{3}$$

$$\frac{\partial(\rho\boldsymbol{V})}{\partial t}+\nabla\cdot(\rho\boldsymbol{V}\boldsymbol{V})=-\nabla p+\nabla\cdot\mu\left[\nabla\boldsymbol{V}+(\nabla\boldsymbol{V})^T\right]-\sigma\int k\boldsymbol{n}\delta\left(\boldsymbol{x}-\boldsymbol{x}_f\right)dA, \tag{4}$$

where $\boldsymbol{V}$ is the velocity vector, ρ is the density, p is the pressure, μ is the viscosity, σ is the surface tension coefficient, k is twice the local mean curvature, $\boldsymbol{n}$ is a unit vector outwardly normal to the local surface, and $\boldsymbol{x}$ is the space vector with the subscript "f" denoting the interface. It is seen that surface tension is implanted as a delta function integrated locally over the immiscible interface so as to render a singular force exerted on the flow field. The present study considers only

head-on collisions of droplets (i.e., $B = 0$), which are intrinsically axisymmetric with respect to the axis connecting the two centers of mass of the droplets. Consequently, the axisymmetric versions of Eqs. (3) and (4) were used in the present study.

All the variables in the simulation are nondimensional. Specifically, the governing equations are non-dimensionalized by using the radius of the smaller droplet R_s (degenerate to R for equal-size droplets), the relative velocity U, and the liquid density ρ_l. The Weber number is defined by $We = 2\rho_l U^2 R_S/\sigma$, where σ is the gas-liquid surface tension coefficient. The size ratio is defined by $\Delta = R_L/R_S$, where R_L is the radius of the larger droplet. The Ohnesorge number is defined by $Oh = 16\mu_l(\rho_l R_S \sigma)^{-1/2}$, where μ_l is the liquid viscosity. The liquid Reynolds number is defined by $Re_l = 2\rho_l U R_S/\mu_l = 16\sqrt{2We}/Oh$. The density ratio, ρ_g/ρ_l, and the viscosity ratio, μ_g/μ_l, are two or three orders of magnitude smaller than unity, and therefore, their effects on the droplet deformation and viscous dissipation can be neglected as confirmed by many previous studies.[15,16,39,40]

A cylindrical coordinate (r, z) is established so that the connection of the mass center for the droplets forms the radial direction, r, and the axial direction, z, is perpendicular to it, as shown in Fig. 1. The velocity component in the radial and axial directions is u and w, respectively. The axisymmetric domain of $16R_L$ in length and $3R_L$ in radius is discretized by a uniform, orthogonal staggered mesh. Slip velocity boundary conditions are specified to all the boundaries except the axis, where the axisymmetric boundary condition is specified.

In the present simulation, the larger droplet was set as being initially stationary, while the smaller droplet was set to be with an initial velocity (i.e., the relative velocity) corresponding to a given collision Weber number. According to the experiments that were used to validate the present simulation in Subsections II B and II C, water or n-tetradecane droplets of $O(10^2)$ μm were used, and the relative velocity was about O(1) m/s. It should be noted that the velocity of the center of mass of the binary system has been subtracted from the result analysis.

B. Grid-dependence analysis

For the present grid-dependence analysis, five grids were generated by specifying different grid nodes in the r-direction (N_r) and the z-direction (N_z), with the total number of nodes being $N_r \times N_z$. We considered a representative case of equal-size droplet bouncing at $We = 2.3$ and $Oh = 0.594$ and examined the grid-dependence of droplet deformation and droplet kinetic energy on the grid resolution.

Figure 2(a) shows the evolution of simulated droplet deformation and Fig. 2(b) shows that of the simulated droplet kinetic energy for five different meshes from the coarsest one, 66×121, to the finest one, 88×968. In terms of droplet deformation for qualitative comparison, all the meshes produce almost identical results during the entire collision process except the coarsest grid of 66×121, which causes slight discrepancy from the others. In terms of droplet kinetic energy for quantitative comparison, all the meshes again produce almost the same results throughout most of the collision process before $T = 1.4$, when the droplets have started bouncing back. Except the coarsest grid of 66×121, which moderately underestimates the droplet kinetic energy after $T = 1.4$, the other predictions differ from each other by less than 15%, and the grid-dependence is substantially decreased for the grids finer than 88×242. Recognizing that the finest mesh of 88×968 demands significantly longer computation time than the others; the present study adopted the mesh of 88×484 to balance computation load and accuracy. A typical run with the grid of 88×484 for $T = 2.0$ takes about half an hour on an Intel Xeon E5 2692 central processing unit (CPU).

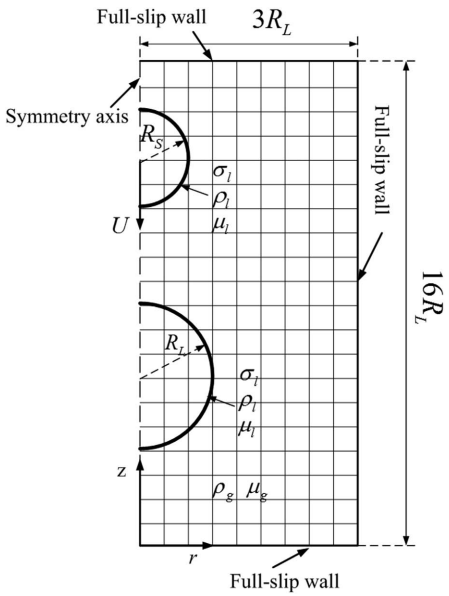

FIG. 1. Axisymmetric computational domain, uniform structured grids, and boundary conditions. A coarse mesh of 8×19 is shown for schematic.

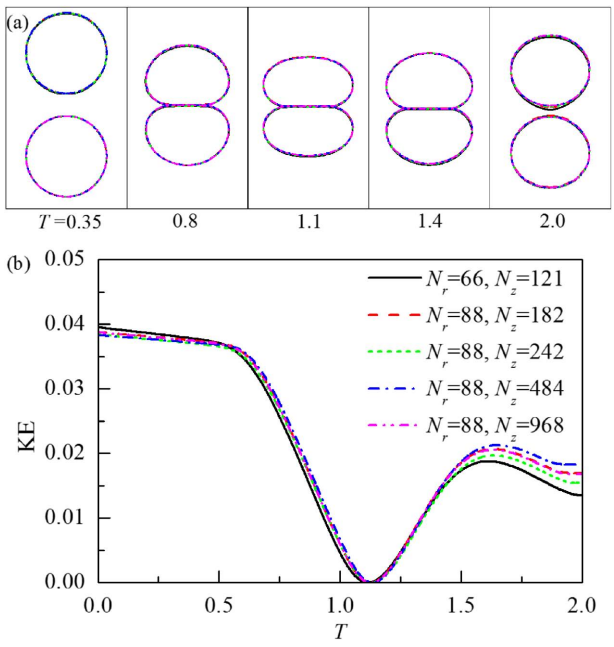

FIG. 2. Grid-dependence of (a) droplet deformation and (b) droplet kinetic energy (KE) for droplet bouncing at $\Delta = 1.0$, $We = 2.3$, and $Oh = 0.594$.

Furthermore, it has been recognized that the front tracking method adopted in the present study is not sensitive to the grid size[41] because the interface is represented by massless Lagrangian points without shape or size and therefore does not require extremely refined mesh. This is one of the advantages of the front tracking method compared with those resolution-demanding VOF (volume-of-fluid) and level-set methods.

C. Experimental validation

To validate the present simulation, we adopted the experimental results of Pan *et al.*[16] on head-on collisions of n-tetradecane droplets. In their paper, high-quality time-resolved shadowgraph images are available. It is noted that the earlier experimental results of Jiang *et al.*[5] and Qian and Law[6] have been extensively used for validating interface-capturing numerical methods, but their relatively low spatial resolutions alleviate the difficulty of achieving good agreement between the simulation and the experiment. The validation against the experimental results of Pan *et al.*[16] is significantly more challenging because of the great details about the droplet deformation to be captured.

It is noted that the bouncing regime (II) is located between two coalescence regimes (I) and (III) in a *We-B* nomogram. For convenience, the collisions near the transition between regimes (I) and (II) are referred to as "soft" collisions with moderate droplet deformation and those near the transition between regimes (II) and (III) as "hard" collisions with substantial droplet deformation.[16] Consequently, both "soft" and "hard" collisions were considered in the present validation.

Figure 3(a) compares the experimental and simulated evolution of droplet deformation for the "soft" bouncing of equal-size n-tetradecane droplets at $We = 2.3$ and $Oh = 0.594$. The natural oscillation[42] of the smaller droplet, defined by $\tau = \pi(2\rho_l R_s^3/\sigma)^{1/2}/4$, was often used as a characteristic time in droplet-related studies and therefore is also given as a reference time scale in the present simulation. The characteristic time introduced in the non-dimensionalization of the governing equations is related to the natural oscillation time by $D_s/U = 4\pi^{-1}We^{-1/2}\tau$. Consequently, the nondimensional time is $T = 2R_s/Ut$, where t is real time.

To facilitate the quantitative comparison, the simulated droplet contours were selected at the same dimensional time instants when the experimental images are available. Furthermore, the simulated droplet contours are superimposed on the experimental images so that any discrepancies between them are manifest. It is seen that the simulation shows very good agreement with the experiment in terms of droplet deformation throughout the entire collision process.

Figure 3(b) shows the case of "hard" bouncing at $We = 9.3$ and $Oh = 0.598$, where the experimental droplets are slightly smaller than those in the case shown in Fig. 3(a) and therefore result in a slightly larger Ohnesorge number. Again, very good agreement between the experimental and simulation results can be observed. It is also seen that the droplets undergo substantially larger deformation at the higher Weber number since the Ohnesorge numbers are close in the two cases. The two validation cases demonstrate that the present numerical methods can accurately predict the evolution of droplet deformation during the bouncing processes.

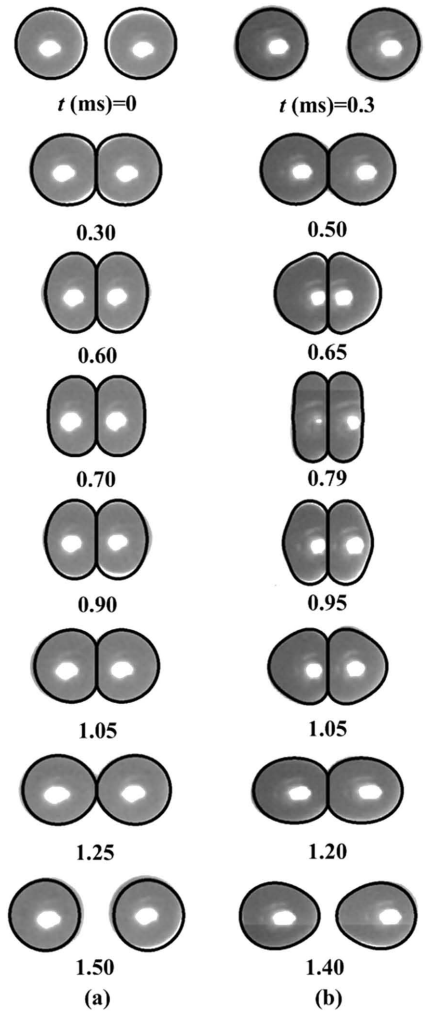

FIG. 3. Time sequences of droplet bouncing from the experimental images[16] (shadow graphs) and the present simulation results (thick solid lines) for equal-size n-tetradecane droplets at atmospheric pressure. (a) $\Delta = 1.0$, $We = 2.3$, and $Oh = 0.594$; $R = 170.6\ \mu$m; and $T_0 = 0.831$ ms, (b) $\Delta = 1.0$, $We = 9.3$, and $Oh = 0.598$; $R = 167.6\ \mu$m; and $T_0 = 0.811$ ms. Reproduced with permission from Pan *et al.*, "Experimental and mechanistic description of merging and bouncing in head-on binary droplet collision," J. Appl. Phys. **103**, 064901 (2008). Copyright 2008 AIP Publishing LLC.

III. RESULTS AND DISCUSSION

A. Bouncing of unequal-size droplets

Tang *et al.*[8] experimentally studied the head-on collision of unequal-size n-tetradecane droplets and presented a number of high-quality experimental shadowgraph images, which however have not been numerically reproduced. Figure 4 presents the comparison between the experiment images and the simulated droplet contours at $We \approx 7.3$, $Oh = 0.775$, and $\Delta = 1.46$, 1.87, and 2.33. An equal-size bouncing case from the study of Tang *et al.*[8] at $We = 8.5$ and the same Ohnesorge number is also shown in Fig. 4(a). To facilitate the direct comparison between the experiment and simulation, the simulated droplet contours were selected at the same dimensional time instants when the experimental images are available.

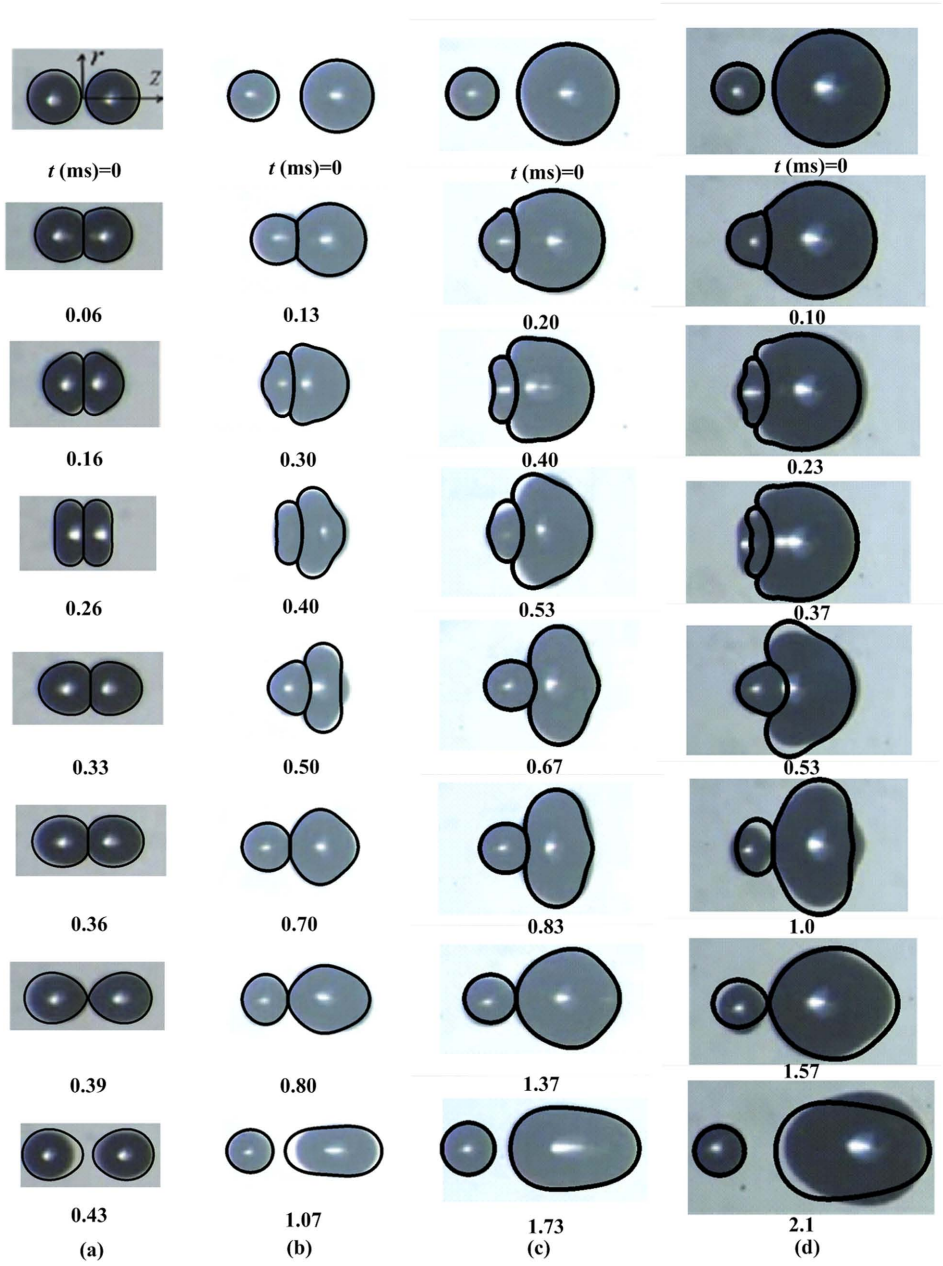

FIG. 4. Time sequences of droplet bouncing from the experimental images[8] (shadow graphs) and the present simulation results (thick solid lines) for equal-size n-tetradecane droplets at atmospheric pressure. (a) Δ = 1.0, *We* = 8.5, (b) Δ = 1.46, *We* = 7.3, (c) Δ = 1.87, *We* = 7.3, and (d) Δ = 2.33, *We* = 7.0. *Oh* = 0.775; R_s = 100 μm; and T_0 = 0.376 ms. Reproduced with permission from Tang *et al.*, "Bouncing, coalescence, and separation in head-on collision of unequal-size droplets," Phys. Fluids **24**, 022101 (2012). Copyright 2012 AIP Publishing LLC.

Overall, the numerical predictions agree well with experimental results throughout the entire collision process, again substantiating the applicability of the present numerical methodology in simulating droplet bouncing. The discrepancies between the simulation and the experiment may be attributed to the imperfect experimental conditions to be specified as follows.

For the equal-size droplet bouncing shown in Fig. 4(a), the simulation precisely predicts the experimental droplet contours except that at t = 0.43 ms, when the experimental image shows slightly asymmetric droplet deformation as such the left droplet is almost spherical while the right one is not. The small experimental error may be caused by the unavoidable disturbance of ambient gas flow to the droplets as small as 100 μm.

For the unequal-size droplet bouncing at Δ = 1.46, shown in Fig. 4(b), the numerical predictions also show very good agreement with the experimental images not only for the deformation of the smaller droplet but also for that of the larger droplet. Small discrepancies can be found at t = 0.50 ms and t = 1.07 ms, and they are probably caused by the experimental uncertainties in temporal resolution. It is noted that the temporal uncertainty of collision images in the experiment of Tang *et al.* is approximately 0.1 ms in the early stage of droplet collision and can be as large as 20%–30% in the late stages.[8,20] The same explanation can be applied to the droplet bouncing at Δ = 1.87, shown in Fig. 4(c), where all the experimental images are predicted well by the simulation except the one at t = 0.53.

Relatively large disagreement between the simulation and experiment is found for the droplet bouncing at Δ = 2.33, shown in Fig. 4(d). After the initial interaction, the simulated droplets show slightly larger deformation than the experimental ones. Two experimental issues can be considered to cause the slight disagreement. First, both the experimental images and the simulated droplet contours show that, with increasing

Δ by fixing R_S while increasing R_L, the larger droplet requires a longer time to reach its maximum deformation than the smaller droplet does. The prolonged collision process may cause larger experimental uncertainties in time as discussed above. Second, it is increasingly difficult to experimentally realize the head-on collision of unequal-size droplets with increasing Δ because the droplets can be easily off-center in the direction perpendicular to the image plane.

The above discussions about the imperfections of the experiments do not rule out the possible computational errors. For example, the numerical errors associated with solving the governing equation by using the 2nd-order finite difference method may also cause errors in the velocity field and then tracking the Lagrangian droplet interface. The large liquid-gas density ratio[43] and the extremely thin gas film[44] between two colliding droplets are other possible causes for numerical uncertainty and require more sophisticated numerical schemes.[45]

B. Boundary-layer-like droplet internal flow

The significance of viscous dissipation in affecting droplet collision outcomes has been recognized by previous studies.[5,6,8,10,15] Specifically, the rapid droplet deformation in the early stage of droplet collision induces a strong droplet internal flow and hence high viscous dissipation rates. The accumulated viscous dissipation reduces the effective droplet kinetic energy for droplet coalescence and therefore promotes droplet bouncing.[15]

Inspired by von Kármán's classical theory on rotating-disk flow, Zhang and Law[15] proposed an analytically tractable model for the droplet internal flow induced by the approximately flattened, outwardly expanding droplet interfaces. The velocity components for the axisymmetric flow are given by

$$u = \frac{1}{2}\nu_l \eta^2 r e^{-\eta z}, \quad w = -\nu_l \eta (1 - e^{-\eta z}), \tag{5}$$

where $\eta = 1.503(\kappa/\nu_l)^{1/2}$, κ is the strain rate, and $\nu_l = \mu_l/\rho_l$ the kinematic viscosity of the liquid. In the early stage of droplet collision, the rapid droplet deformation results in large κ and therefore large η. Consequently, the flow resembles a boundary-layer-like one, and $1/\eta << R$ represents the characteristic length of the boundary layer, beyond which the viscous dissipation can be neglected. Although Eq. (5) has been found to yield reasonable estimations to the viscous dissipation within the droplet, it has not been explicitly validated by either experiment or simulation. The numerical simulation of Pan *et al.*[16] on the head-on collision of equal-size droplets shows that the velocity gradient near the colliding interface is much larger than that inside the droplet, but no details about its physical implications were given. In the present study, the instantaneous, local viscous dissipation rate is calculated by[46]

$$\Phi = \mu\left[2\left(\frac{\partial u}{\partial r}\right)^2 + 2\left(\frac{u}{r}\right)^2 + 2\left(\frac{\partial w}{\partial z}\right)^2\right] + \mu\left(\frac{\partial u}{\partial z} + \frac{\partial w}{\partial r}\right)^2 - \frac{2}{3}\mu\left[\frac{1}{r}\frac{\partial (ru)}{\partial r} + \frac{\partial w}{\partial z}\right]^2, \tag{6}$$

where the last item vanishes for incompressible flows. In the following discussion, the non-dimensional Φ is denoted by the viscous dissipation rate (VDR) for short.

We compared the numerical results and theoretical estimations of Zhang *et al.*[15] for the streamlines and the VDR contours at selected times in the early stage for a hard collision at $We = 7.3$ and $Oh = 0.775$, as shown in Fig. 5. Several observations can be made from the comparison as follows. First, regardless of some discrepancies to be discussed, the theoretical estimation qualitatively agrees with the simulation in terms of the VDR distribution and the instantaneous streamlines. Second, notable viscous dissipation is concentrated in a very thin layer near the colliding interface, where large strain rates can be found, as clearly shown in the amplified VDR contours in the layer. Third, the numerical VDR distribution is not uniform at $T = 0.09$ as it slightly increases from the interface center to the interface rim, where the flow has higher local strain rates. This is however not predicted by the theoretical estimation because the theory idealizes the outwardly expanding interface as a sufficiently large one and hence ignores the boundary effect around the interface rim. Finally, the colliding interfaces slowly approach to each other after the early stage,

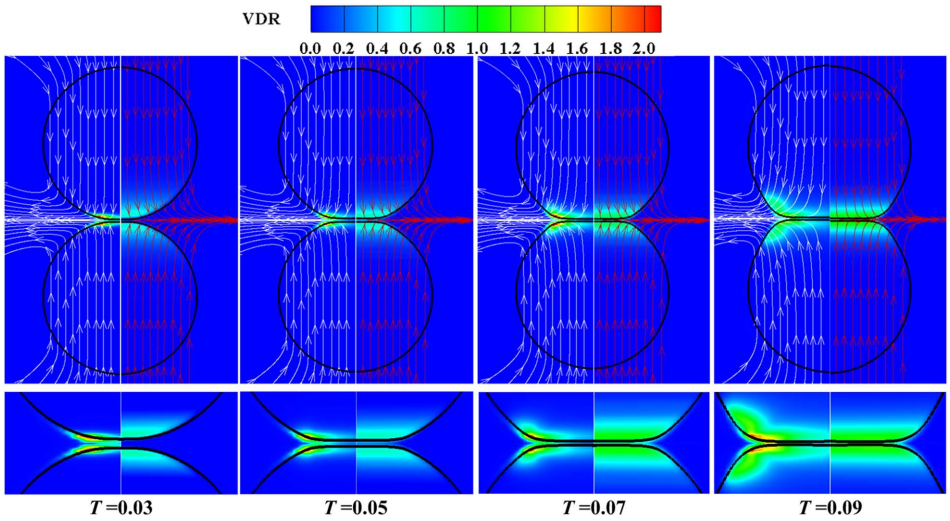

FIG. 5. Viscous dissipation rate (VDR) contours and instantaneous streamlines from the present simulation results (on the left half) and the theoretical analysis of Zhang and Law[15] (on the right half) for the case of "hard" droplet bouncing at $\Delta = 1.0$, $We = 7.3$, and $Oh = 0.775$.

while the droplets continue deforming under their inertia and the high VDR area moves from the vicinity of the colliding interfaces to the droplet interiors.

To further substantiate the boundary-layer-like droplet internal flow, we simulated and showed the case of soft collision at We = 2.3 and Oh = 0.775 in Fig. 6. It is seen that, although the droplet deformation for the soft collision is less intense compared with that for the hard collision, the droplet internal flow induced by the outwardly expanding interfaces still shows the boundary-layer characteristics with the high local strain-rates and hence the high VDRs being concentrated around the colliding interfaces. It is noted that the boundary effect around the interface rim is insignificant for the soft collision because the droplet deformation is small at the small Weber number.

C. Viscous dissipation in bouncing droplets of unequal sizes

The experiment of Tang *et al.*[8] has shown that the size ratio slightly affects the transition Weber number from bouncing (Regime II) to coalescence (Regime III). Figure 7 shows the evolution of various droplet energies during the hard collisions at We = 7.3, Oh = 0.775, and various Δ, all of which result in droplet bouncing. The unequal-size cases (b)–(d) in Fig. 7 correspond to the cases (b)–(d) in Fig. 4, and the equal-size case (a) at the same We and Oh is also shown for comparison. Although the present FTM does not have to solve the energy equation, the total energy (TE), consisting of the kinetic energy (KE), the surface energy (SE), and the dissipation energy (DE), is well conserved throughout the entire collision process and for all the considered cases. To facilitate the following discussion, a bouncing time T_B was defined as the instant when the width of the gas film at the axis is larger than a threshold, say, $h_c = 0.05R_s$, after the maximum droplet deformation. It is noted that droplet T_B increases slightly with Δ, implying that the collision behavior of the smaller droplet may dominate the entire "hard" bouncing process.

The entire droplet deformation can be divided into several distinct stages. The first stage is characterized by the outwardly expanding interfaces that induce a "stagnation-like" droplet internal motion in each droplet. The droplet interiors away from the expanding interfaces are nearly undeformed, as clearly indicated by the almost uniform streamlines. The total viscous dissipation rate (TVDR), calculated by integrating the VDR over the droplets, arrives a peak value at the end of the stage, denoted by T_1, and starts to decrease afterwards. It is noted that the peak TVDR increases with Δ because of the enlarged area with high VDRs around the colliding interfaces, as clearly seen in the VDR contour at time T_1.

The second stage is characterized by the significant deformation of the smaller droplet in contrast to the slight deformation of the larger droplet, where the streamlines remain mostly uniform. As shown at a representative time T_2, the decreased TVDR is mainly distributed in the area away from the colliding interfaces, such as in the "shoulders" of both droplets in case (a) for equal-size collision and in the "shoulder" of the smaller droplet in cases (b)–(d) for unequal-size collisions. At the end of the stage, the TVDR contour has a local minimum, exactly corresponding to the time instant when the equal-size droplets reach their maximum deformation (i.e., the maximum SE). The local minimum of the TVDR appears slightly advance the maximum SE for Δ = 1.46 but significantly prior to those for Δ = 1.87 and Δ = 2.33. This is because the droplets reach their individual maximum deformation at different time instants and the total SE is increasingly determined by the deformation of the larger droplet with increasing Δ.

The third stage is characterized by the significant deformation of the larger droplet and by the bouncing tendency of the smaller droplet, whose streamlines are directed upward. The bouncing smaller droplet causes a local maximum of the TVDR at T_3, and the viscous dissipation is concentrated in the vertex area of the smaller droplet.

The fourth stage is characterized by the bouncing tendency of the larger droplet, which causes another local maximum of TVDR at T_4. It is seen that the streamlines across the larger droplet are directed downward. Similar local maximum of the TVDR does not appear in the equal-size case because the identical droplets start bouncing back at the same time instant. The final stage is the eventual bouncing of the droplets after T_4.

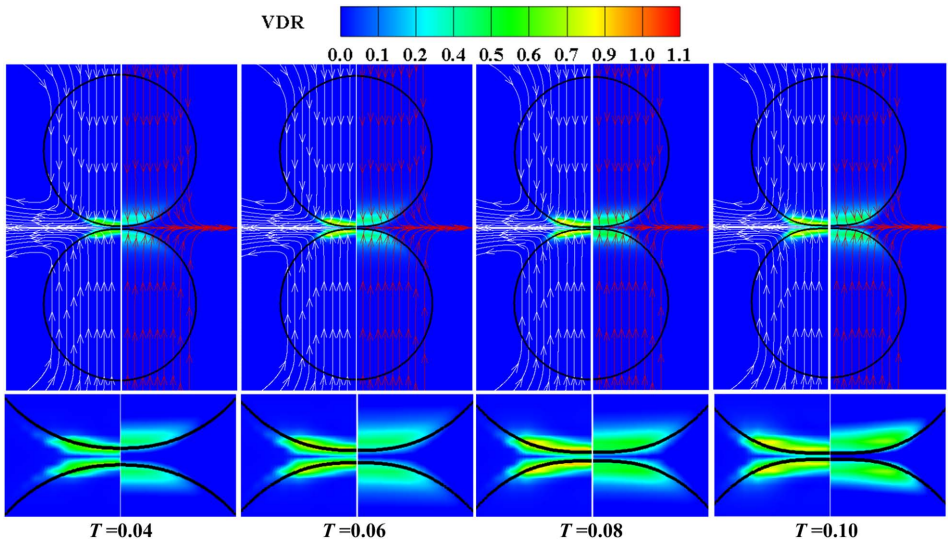

FIG. 6. Viscous dissipation rate (VDR) contour and instantaneous streamlines from the present simulation results (on the left half) and the theoretical analysis of Zhang and Law[15] (on the right half) for the case of "soft" droplet bouncing at Δ = 1.0, We = 2.3, and Oh = 0.775.

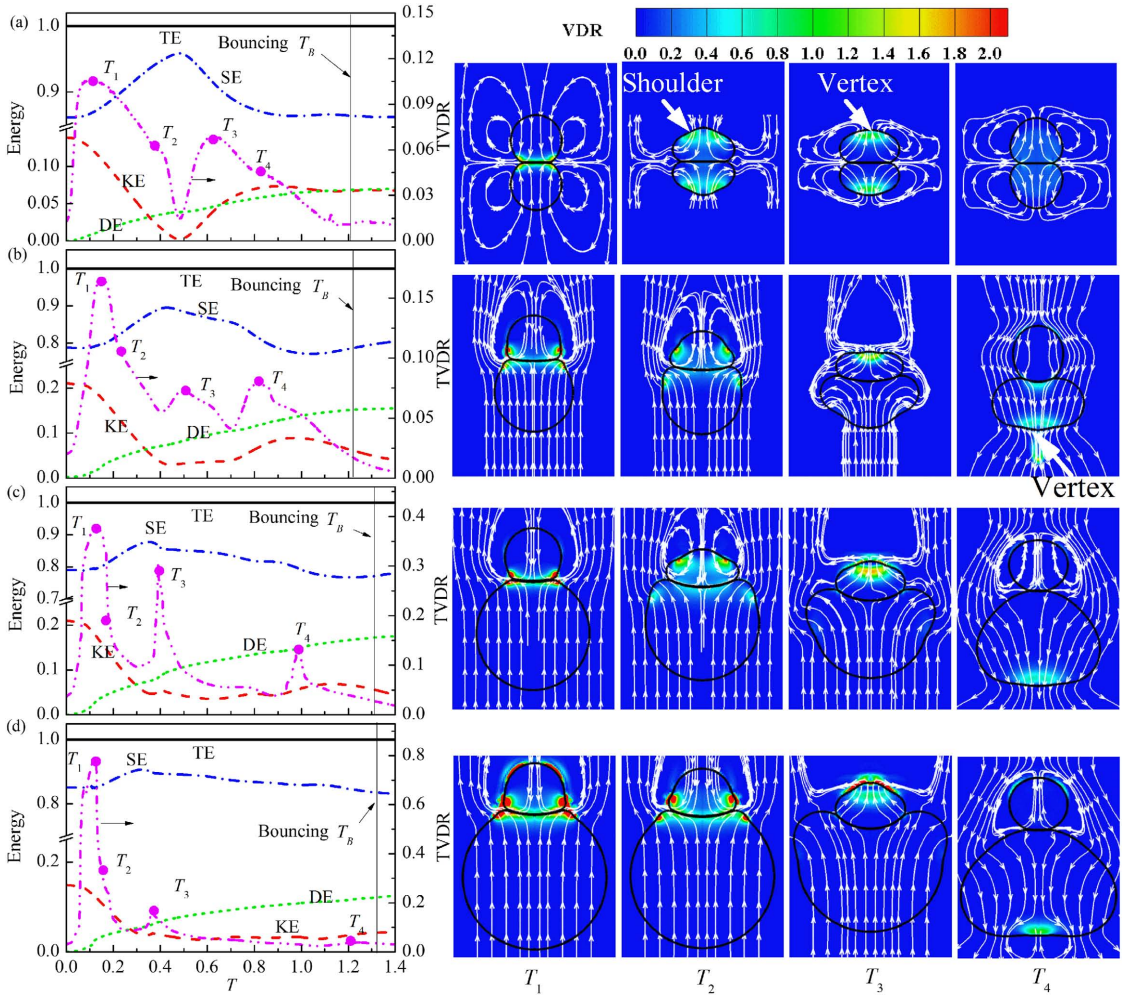

FIG. 7. Evolution of various energies of the droplets during the "hard" droplet bouncing under atmospheric pressure at $We = 7.3$, $Oh = 0.775$ and (a) $\Delta = 1.0$, (b) $\Delta = 1.46$, (c) $\Delta = 1.87$, and (d) $\Delta = 2.33$, which correspond to those in Fig. 4. The total kinetic energy (KE), the total dissipation energy (DE), the surface energy(SE), the total energy (TE), and the total viscous dissipation rate (TVDR) of the droplets, which are normalized by the initial total energy of the droplets. Local viscous dissipation rate (VDR) contours and instantaneous streamlines are shown at selected times in the right graphs.

Time-dependent DE(T) is calculated by integrating the TVDR over the nondimensional time. It is interesting to observe that DE(T_B), which is the accumulated DE at the bouncing time, first increases then decreases with increasing Δ and reaches its peak value at about $\Delta = 1.87$. This can be understood by recognizing that DE(T_B) is linearly proportional to the energy dissipation fraction f_E by $f_E = 1 - (KE'/KE) = DE(T_B)/KE$. Either the previous empirical formula proposed by O'Rourke, Eq. (2), or the fitting formula to be shown shortly in Sec. III D implies the possibility of such a nonmonotonicity. The physical reason is that, for unequal-size droplet collision, the correct measure of the relative importance of the kinetic energy compared with the surface energy is $We^*_{cr} = We_{cr}\Delta^3/[12(1+\Delta^3)(1+\Delta^2)]$, which is a nonlinear function of Δ.[12] Moreover, the prominent peak values of the VDR at T_3 and T_4 for $\Delta = 1.87$ and $We = 7.3$ can be understood by that the strong internal motions are induced by the droplet deformation at the size ratio and the Weber number, which also result in the peak value of DE(T_B), as we discussed earlier.

To further investigate the viscous dissipation during droplet bouncing, we extended the above discussion to the soft bouncing at $We = 2.3$. It is noted that the experimental results reported in Tang *et al.*[8] for the transition from coalescence (Regime I) to bouncing (Regime II) also suggest the tendency of droplet bouncing with increasing Δ to being less than 3.0. Because the collision at $We = 2.3$ and $\Delta = 1.0$ results in bouncing, as observed by Pan *et al.*,[16] droplet bouncing at the same Weber number and larger Δs are expected to happen.

Figure 8 show the energy budget and VDR contour for the soft bouncing at $We = 2.3$, $Oh = 0.775$, and $\Delta = 1.0$, 1.46, 1.87, and 2.33. Several observations can be made about the simulations. First, the total energy is well conserved and the boundary-layer-like droplet internal flow is also confirmed. Second, all the droplet deformation stages of hard collision can be found for their counterparts in the soft collisions although the latter ones have smaller deformation because of the smaller Weber number. Third, the local maximum TVDR increases with Δ, but the increase is far less than that in the hard collision. Fourth, the droplet bouncing time slightly decreases with Δ, implying the increasing influence of the surface energy of the larger droplet at the small Weber number.

An interesting observation can be found in cases (c) and (d), where the larger droplet starts to bounce off prior to the

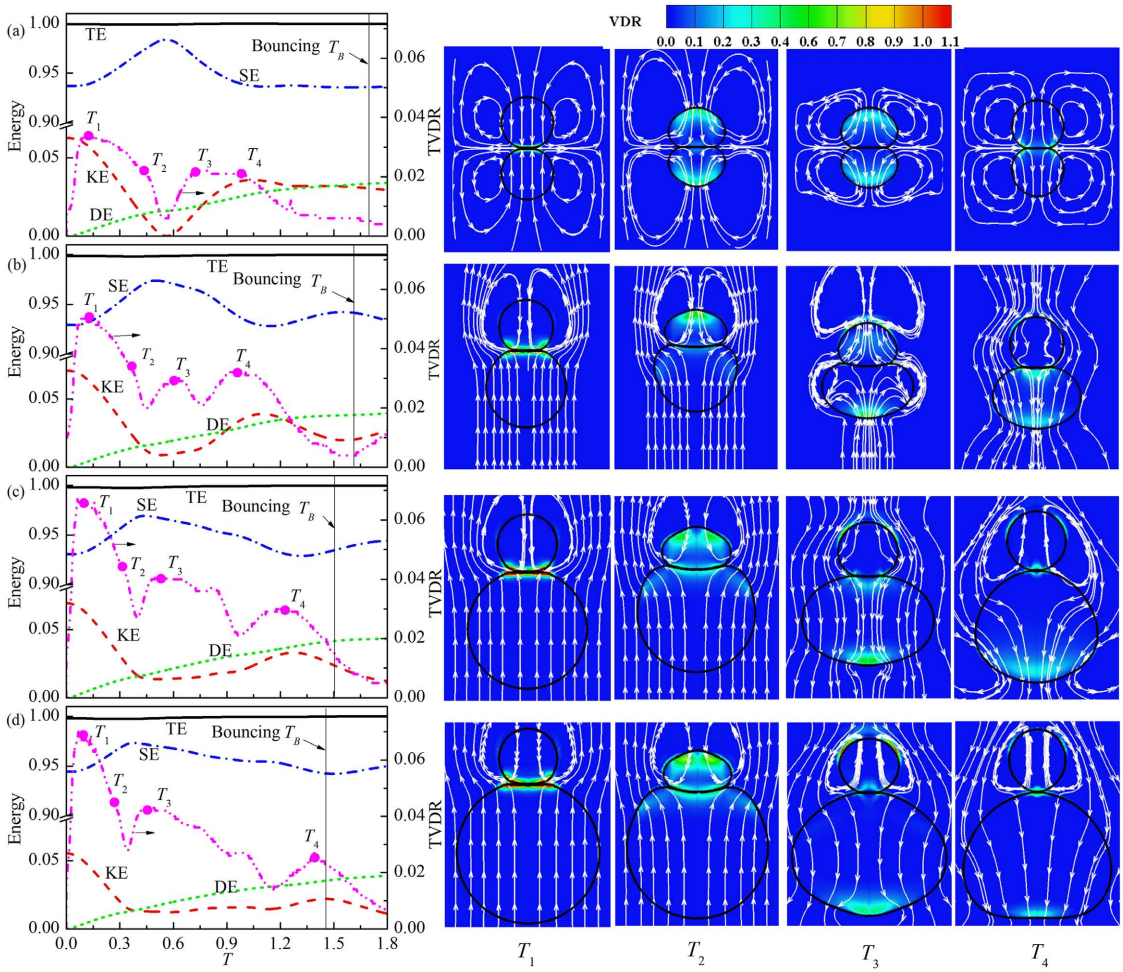

FIG. 8. Evolution of various energies of the droplets during the "soft" droplet bouncing under atmospheric pressure at We = 2.3, Oh = 0.775 and (a) Δ = 1.0, (b) Δ = 1.46, (c) Δ = 1.87, and (d) Δ = 2.33. The notations are the same as those used in Fig. 7.

smaller one, as seen at the representative time T_3. To understand this, we noted that the surface energy plays a dominant role in the energy budget of droplet collision at small We and with increasing Δ. Consequently, in the soft collision cases with large Δ, the kinetic energy of the larger droplet is relatively too small to have a significant influence in the collision process, and the larger droplet has a smaller deformation and tends to recover its spherical shape earlier than the smaller droplet. In addition, the nonmonotonic trend of DE(T_B) is insignificant for the soft collision, where DE(T_B) remains almost constant with increasing Δ.

D. Kinetic energy recovery of bouncing droplets

To make the above results on inelastic droplet bouncing practically useful for Lagrangian spray simulation, we conducted a comprehensive parametric study on the influence of We, Δ, and Oh on the kinetic energy recovery factor, $1 - f_E$, or more conveniently on the energy dissipation fraction, f_E. The objective of the study is to derive a fitting formula for f_E, which should be physically meaningful and based on the simulation results.

Figure 9 is used to show that the proposed formula ($f_E - f_{E,cr}$)/($We^* - We_{cr}^*$) correctly includes the effect of the size ratio and therefore can be used to directly compare the results for different size ratios. To derive such a fitting formula, we first recognized that a Δ–weighted Weber number, We^*, should be used to replace the Weber number, We, in the energy analysis,

$$We^* = \frac{\Delta^3}{12(1+\Delta^3)(1+\Delta^2)} We. \tag{7}$$

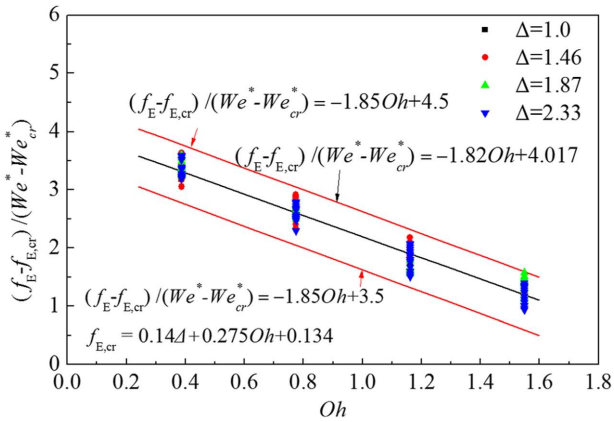

FIG. 9. Variation of the energy dissipation fraction, f_E, with the modified Weber number, $We^* = We\Delta^3/[12(1+\Delta^3)(1+\Delta^2)]$. Symbols denote the simulated data and solid lines denote the linear correlations.

The modified Weber number was first proposed by Rabe *et al.*[12] to measure the relative importance of the total kinetic energy of two droplets compared with their total surface energy. By using the modified Weber number, the results for different size ratios can be directly compared with each other.

Inspired by the experimental observation of Jiang *et al.*[5] that the total viscous dissipation is a linear function of the Ohnesorge number, we proposed the fitting formula as

$$\frac{f_E - f_{E,cr}}{We^* - We^*_{cr}} = c_1 Oh + c_2, \tag{8}$$

where $We^*_{cr} = We_{cr}\Delta^3/[12(1+\Delta^3)(1+\Delta^2)]$ and We_{cr} is the critical Weber number between regimes (I) and (II) for head-on collisions. For tetradecane droplet collision at atmospheric pressure, $We_{cr} = 2.26$ has been experimentally determined.[6] Equation (8) reflects the experimental observation that f_E increases with We^* because higher We^* results in larger droplet deformation and higher kinetic energy loss due to viscous dissipation. The inclusion of $f_{E,cr}$ and $We_{cr}{}^*$ accounts for the fact the viscous dissipation is nonzero for $We^* < We_{cr}{}^*$, when droplet coalescence occurs.

It is seen in Fig. 9 that all the simulated data are satisfactorily fitted by Eq. (8) with

$$f_{E,cr} = 0.14\Delta + 0.275Oh + 0.134, c_1 = -1.82, c_2 = 4.017, \tag{9}$$

and $R^2 = 0.907$. The dependence of $f_{E,cr}$ on Δ and Oh is expected because the viscous dissipation during the droplet collision (coalescence) below the critical Weber number should also vary with Δ and Oh; the linearity is the result of a best fitting. To examine the sensitivity of the formula on the fitting coefficients, we plotted another two fitting formulas with $c_1 = -1.85$, $c_2 = 3.5$ and $c_1 = -1.85$, $c_2 = 4.5$. It is seen that all the simulated data are located in the area enclosed by the two lines representing the formulas. Because of the paucity of experimental data, the proposed fitting can be considered as practical, nevertheless, physically justifiable approximations for accounting for the energy recovery of bouncing droplets after inelastic head-on collision.

E. Interface hysteresis for hard and soft bouncing

In their numerical simulation of equal-size droplet collision, Pan *et al.*[16] observed an interesting phenomenon that, when the colliding interfaces start bouncing back, the pressure on the gas film side of the interfaces drops so rapidly that the higher pressure on the droplet sides of the interfaces pushes the concave (toward the droplets) interface to be convex (toward the gas film). They also found that the phenomenon occurs

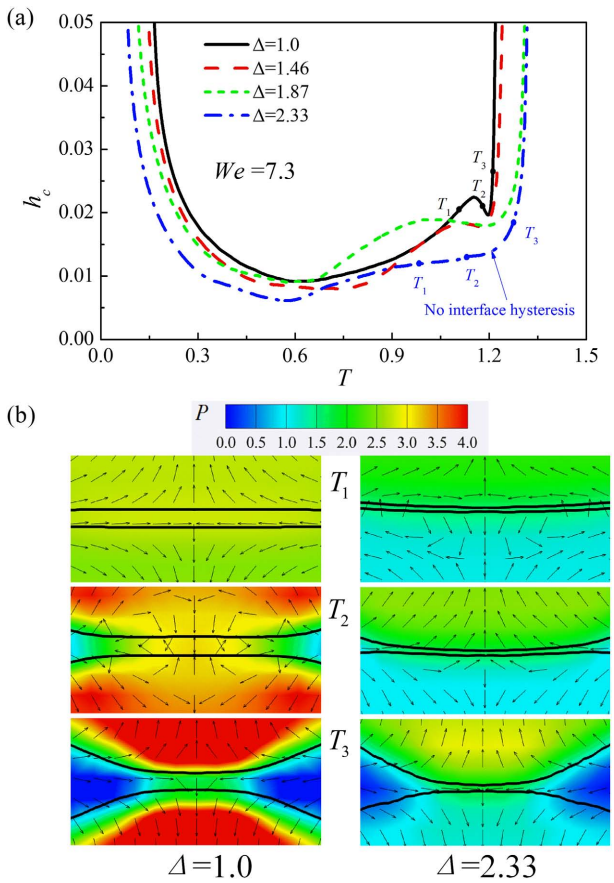

FIG. 10. (a) Evolution of the representative width, h_c, of the gas film between colliding droplets under atmospheric pressure and at various size ratios and fixed $We = 7.3$ and $Oh = 0.775$ and (b) the nondimensional pressure contours and velocity vectors for the cases at $\Delta = 1.0$ and $\Delta = 2.33$.

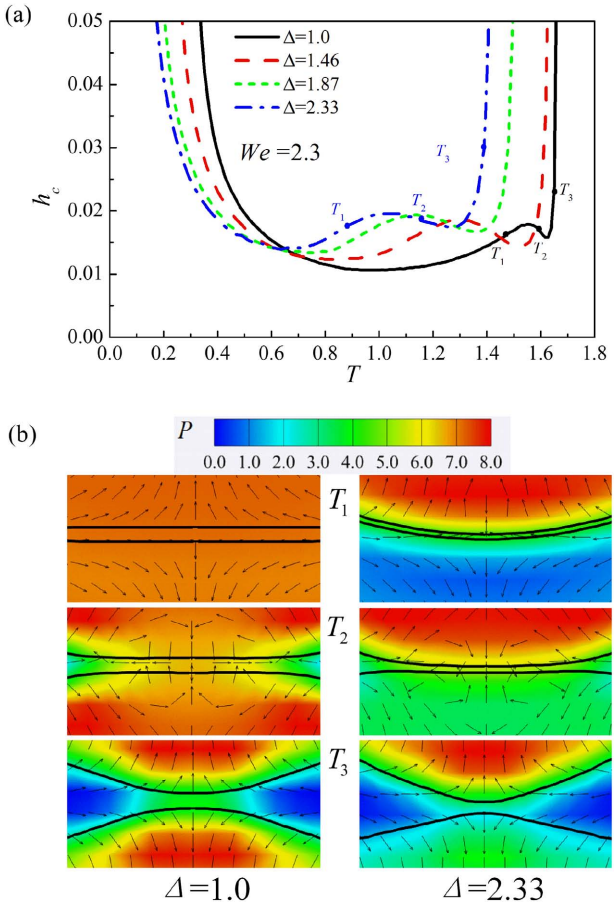

FIG. 11. (a) Evolution of the representative width, h_c, of the gas film between colliding droplets for the "soft" bouncing under atmospheric pressure for various size ratios and fixed $We = 2.3$ and $Oh = 0.775$ and (b) the nondimensional pressure and velocity vectors at the cases of $\Delta = 1.0$ and $\Delta = 2.33$.

not only in soft bouncing but also in hard bouncing. Similar observation can be seen in VOF simulation of Li for equal-size droplet collision.[25] In the present study, we call the interesting but inadequately understood post-collision phenomenon "interface hysteresis," in which the colliding interfaces of two bouncing droplets tend to approach each other for a short period of time when the centers of mass of the droplets have already started to depart from each other.

Figure 10(a) shows the evolution of the gas film thickness at the axis, h_c, at We = 7.3 and various Δs. For the case of Δ = 1, h_c decreases rapidly to a minimum value in the early stage of droplet collision. The minimum h_c decreases with increasing Δ, indicating closer interfaces and larger droplet deformation. Subsequently, instead of monotonically increasing with time, h_c increases to a local maximum, decreases to a local minimum, and then increases again, manifesting the interface hysteresis. The nondimensional pressure ($P = pR_s/2\sigma$) contours and velocity vectors at three representative times during the interface hysteresis, such as T_1, T_2, and T_3, are shown in Fig. 10(b). At T_1, the flows in the droplets direct away from each other and the flow in the gas film is radially inward, indicating the droplets are bouncing off from each other. Such an inward gas flow may cause more rapid pressure drop in the gas film than that in the droplet, and therefore the droplet interfaces are driven by the pressure difference to deform toward another other to new shapes (positions) that satisfy the dynamic boundary condition across the gas-liquid interfaces. It can be seen clearly that, at T_2, the flows in the droplets direct toward each other and the flow in the gas film is radially outward, indicating the droplets are approaching to each other. Once the interfaces find their new balanced shapes and positions, they are dragged to move away from each other again owing to the bouncing droplet masses, as shown in T_3.

The interface hysteresis, which results from the difference between the higher pressure within the liquid droplet and the lower pressure in the gas film, can be observed not only at Δ = 1.0 but also at Δ = 1.46 and 1.87, but it is however absent at Δ = 2.33. To understand this observation, we first noted from Fig. 10(a) that h_c increases more gradually with increasing Δ. The most slowly increasing h_c at Δ = 2.33 cannot result in a rapid pressure drop in the gas film and consequently the interface hysteresis is unlikely to occur.

The tendency of suppressing the interface hysteresis with increasing Δ can also be found for soft collisions at We = 2.3, as shown in Fig. 11. Although, the interface hysteresis can be observed in all four size ratios, the non-monotonic evolution of h_c that indicates the interface hysteresis becomes less prominent with increasing Δ. It is interesting to see that in Fig. 11(b), significantly higher pressure differences are induced at We = 2.3 compared with those at We = 7.3, implying that the interface hysteresis favors smaller droplet deformation at smaller Weber numbers. This is because more slight and symmetric deformation of the colliding droplet promotes the pressure relaxation of the compressed gas film and therefore tends to cause the interface hysteresis.

Viscous dissipation can also promote the interface hysteresis by reducing the droplet deformation. We compared the

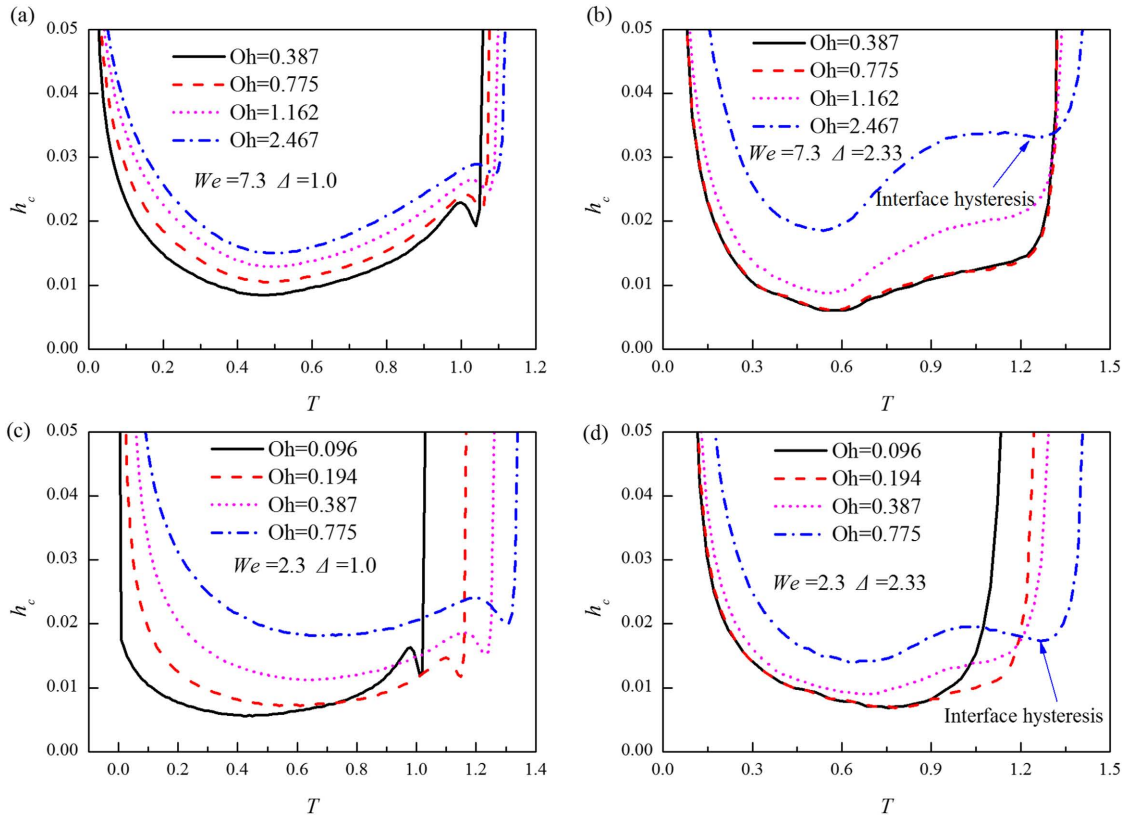

FIG. 12. Influence of the Ohnesorge number, Oh, on the evolution of the gap distance hc at (a) Δ = 1.0 and We = 7.3, (b) Δ = 2.33 and We = 7.3, (c) Δ = 1.0 and We = 2.3, and (d) Δ =2.33 and We = 2.3.

evolution of h_c at different size ratios and different Ohnesorge numbers in Fig. 12, where Oh is varied by changing the liquid viscosity. It is seen that, for equal-size droplet collision at either We = 7.3 or We = 2.3, shown in Figs. 12(a) and 12(c), respectively, the minimum h_c increases with Oh owing to the increasing viscous dissipation and hence reduced kinetic energy for droplet deformation; manifest interface hysteresis can be observed in all the cases in Figs. 12(a) and 12(c). As the size ratio increases to 2.33, as shown in Figs. 12(b) and 12(d), the interface hysteresis emerges only at sufficiently large Oh. Specifically, the interface hysteresis is absent at Oh = 0.387, 0.775, and 1.162 but can be observed at Oh = 2.467 for hard bouncing; it is absent for all the Oh less than 0.096 for soft bouncing.

IV. CONCLUDING REMARKS

A numerical study on the head-on collisions of unequal-size droplets was conducted by using the Front Tracking method (FTM) and sufficiently validated against the high-quality, spatially and temporally resolved shadowgraph images from the experiments of Pan *et al.*[16] and Tang *et al.*[8] The particular interest of the study is to characterize the energy dissipation and interface dynamics of the bouncing droplets upon inelastic head-on collisions.

The first focus of the study is to numerically verify the theoretical hypothesis of Zhang and Law[15] on the concentration of high viscous dissipation rate in the vicinity of colliding interfaces of two identical droplets and to confirm the applicability of the hypothesis to unequal-size droplet collision. The results show that, in the early stage of droplet collision, the droplet deformation is characterized by the rapid outward expansion of colliding interfaces, which induce boundary-layer-like viscous flow and therefore effect concentrated viscous dissipation.

The second focus of the study is to analyze the droplet deformation and energy conversion during droplet collision. In general, the entire droplet bouncing process can be divided into five distinct stages: (I) the early outward expansion of colliding interfaces that induce a boundary-layer-like droplet internal motion in each droplet, (II) the substantial deformation of the smaller droplet, (III) the substantial deformation of the larger droplet and the simultaneous bouncing tendency of the smaller droplet, (IV) the bouncing tendency of the larger droplet, and (V) the eventual bouncing of the droplets. Compared with equal-size droplet collision, unequal-size droplet collision results in increased viscous dissipation, which increases with the size ratio because of the increased area of high strain rates, especially in the early collision stage (I). At smaller Weber numbers and larger size ratios, the surface energy of the larger droplet plays an increasingly important role in the overall energy budget, resulting the interesting phenomenon that the stage (IV) occurs prior to the stage (III).

Motivated by improving the existing model for droplet bouncing in the Lagrangian spray simulation, we conducted the parametric study on the dependence of the energy dissipation fraction, f_E, on various collision parameters such as We, Δ, and Oh. A practically useful and physically meaningful fitting formula was derived as $(f_E - f_{E,cr})/(We^* - We^*_{cr}) = c_1 Oh + c_2$, which was found to well correlate with the numerical results for n-tetradecane droplets. Further validation of the formula against more experimental data is merited in future studies.

The last focus of the study is to investigate the interface hysteresis in stage (V) of droplet bouncing, which occurs when the pressure gradient at the colliding interface reverses its direction and then recovers back. Specifically, the pressure gradient directs from the gas film to the liquid droplet when droplets compress the intervening gas film. During the droplet bouncing, a rapid pressure drop in the gas film, which favors smaller droplet deformation to facilitate the back flow of ambient gas, may reverse the direction of the pressure gradient until the interfaces deform to new balanced shapes. Furthermore, it was found that increasing the Ohnesorge number enhances the interface hysteresis by increasing the viscous dissipation and hence reducing the droplet deformation. By the same reason, increasing the Weber number and the size ratio suppresses the interface hysteresis.

ACKNOWLEDGMENTS

The work was supported by the Hong Kong Research Grants Council/General Research Fund (operating under Contract No. PolyU 152217/14E) and in part by Central Research Grants of the Hong Kong Polytechnic University (operating under Contract Nos. G-UA2M and G-UBGA). The simulations were conducted using the resources of the Tianhe-2 supercomputer. We thank Dr. Xi Xia for stimulating discussions and Mr. Chengming He for code debugging.

[1] C. K. Law, *Combustion Physics* (Cambridge University Press, New York, 2010).
[2] R. Gunn, "Collision characteristics of freely falling water drops," Science **150**, 695 (1965).
[3] P. Brazier-Smith, S. Jennings, and J. Latham, "The interaction of falling water drops: Coalescence," Proc. R. Soc. London, Ser. A **326**, 393 (1972).
[4] N. Ashgriz and J. Poo, "Coalescence and separation in binary collisions of liquid drops," J. Fluid Mech. **221**, 183 (1990).
[5] Y. Jiang, A. Umemura, and C. Law, "An experimental investigation on the collision behaviour of hydrocarbon droplets," J. Fluid Mech. **234**, 171 (1992).
[6] J. Qian and C. Law, "Regimes of coalescence and separation in droplet collision," J. Fluid Mech. **331**, 59 (1997).
[7] J.-P. Estrade, H. Carentz, G. Lavergne, and Y. Biscos, "Experimental investigation of dynamic binary collision of ethanol droplets–A model for droplet coalescence and bouncing," Int. J. Heat Fluid Flow **20**, 486 (1999).
[8] C. Tang, P. Zhang, and C. K. Law, "Bouncing, coalescence, and separation in head-on collision of unequal-size droplets," Phys. Fluids **24**, 022101 (2012).
[9] M. Orme, "Experiments on droplet collisions, bounce, coalescence and disruption," Prog. Energy Combust. Sci. **23**, 65 (1997).
[10] C. Gotaas, P. Havelka, H. A. Jakobsen, H. F. Svendsen, M. Hase, N. Roth, and B. Weigand, "Effect of viscosity on droplet-droplet collision outcome: Experimental study and numerical comparison," Phys. Fluids **19**, 102106 (2007).
[11] F. Y. Testik, "Outcome regimes of binary raindrop collisions," Atmos. Res. **94**, 389 (2009).
[12] C. Rabe, J. Malet, and F. Feuillebois, "Experimental investigation of water droplet binary collisions and description of outcomes with a symmetric Weber number," Phys. Fluids **22**, 047101 (2010).
[13] A. Gopinath and D. L. Koch, "Collision and rebound of small droplets in an incompressible continuum gas," J. Fluid Mech. **454**, 145 (2002).
[14] G. A. Bach, D. L. Koch, and A. Gopinath, "Coalescence and bouncing of small aerosol droplets," J. Fluid Mech. **518**, 157 (2004).

[15]P. Zhang and C. K. Law, "An analysis of head-on droplet collision with large deformation in gaseous medium," Phys. Fluids **23**, 042102 (2011).
[16]K.-L. Pan, C. K. Law, and B. Zhou, "Experimental and mechanistic description of merging and bouncing in head-on binary droplet collision," J. Appl. Phys. **103**, 064901 (2008).
[17]D. Liu, P. Zhang, C. K. Law, and Y. Guo, "Collision dynamics and mixing of unequal-size droplets," Int. J. Heat Mass Transfer **57**, 421 (2013).
[18]J. Eggers, J. R. Lister, and H. A. Stone, "Coalescence of liquid drops," J. Fluid Mech. **401**, 293 (1999).
[19]L. Duchemin, J. Eggers, and C. Josserand, "Inviscid coalescence of drops," J. Fluid Mech. **487**, 167 (2003).
[20]C. Tang, J. Zhao, P. Zhang, C. K. Law, and Z. Huang, "Dynamics of internal jets in the merging of two droplets of unequal sizes," J. Fluid Mech. **795**, 671 (2016).
[21]M. Motzigemba, N. Roth, D. Bothe, H.-J. Warnecke, J. Pruss, K. Wielage, and B. Weigand, "The effect of non-Newtonian flow behaviour on binary droplet collisions: VOF-simulation and experimental analysis," in Proceedings of the 18th International Conference on Liquid Atomization and Spray Systems, edited by A. Lozano (ILASS Europe, Zaragoza, 2002), pp. 559–564.
[22]K. Sun, P. Zhang, C. K. Law, and T. Wang, "Collision dynamics and internal mixing of droplets of non-Newtonian liquids," Phys. Rev. Appl. **4**, 054013 (2015).
[23]K. Sun, T. Wang, P. Zhang, and C. K. Law, "Non-Newtonian flow effects on the coalescence and mixing of initially stationary droplets of shear-thinning fluids," Phys. Rev. E **91**, 023009 (2015).
[24]J. B. Greenberg, "Droplet size distribution effects in an edge flame with a fuel spray," Combust. Flame **179**, 228 (2017).
[25]J. Li, "Macroscopic model for head-on binary droplet collisions in a gaseous medium," Phys. Rev. Lett. **117**, 214502 (2016).
[26]Y. R. Zhang, X. Z. Jiang, and K. H. Luo, "Bounce regime of droplet collisions: A molecular dynamics study," J. Comput. Sci. **17**, 457 (2016).
[27]Z. Zhang, Y. Chi, L. Shang, P. Zhang, and Z. Zhao, "On the role of droplet bouncing in modeling impinging sprays under elevated pressures," Int. J. Heat Mass Transfer **102**, 657 (2016).
[28]N. Nordin, "A mesh independent collision condition for Lagrangian sprays," in *Thermo and Fluid Dynamics* (Chalmers University of Technology, 2000).
[29]J. Zhang, J. Mi, and H. Wang, "A new mesh-independent model for droplet/particle collision," Aerosol Sci. Technol. **46**, 622 (2012).
[30]O. O. Taskiran and M. Ergeneman, "Trajectory based droplet collision model for spray modeling," Fuel **115**, 896 (2014).
[31]F. Perini and R. D. Reitz, "Improved atomization, collision and sub-grid scale momentum coupling models for transient vaporizing engine sprays," Int. J. Multiphase Flow **79**, 107 (2016).
[32]P. J. O'Rourke, *Collective Drop Effects on Vaporizing Liquid Sprays* (Princeton University, New Jersey, 1981).
[33]P. J. Tennison, T. L. Georjon, P. V. Farrell, and R. D. Reitz, "An experimental and numerical study of sprays from a common rail injection system for use in an HSDI diesel engine," SAE No. 980810, 1998.
[34]A. Munnannur, *Droplet Collision Modeling in Multi-dimensional Engine Spray Computation* (University of Wisconsin-Madison, 2007).
[35]A. Munnannur and R. D. Reitz, "A new predictive model for fragmenting and non-fragmenting binary droplet collisions," Int. J. Multiphase Flow **33**, 873 (2007).
[36]S. Kim, D. J. Lee, and C. S. Lee, "Modeling of binary droplet collisions for application to inter-impingement sprays," Int. J. Multiphase Flow **35**, 533 (2009).
[37]A. Munnannur and R. D. Reitz, "Comprehensive collision model for multidimensional engine spray computations," Atomization Sprays **19**, 597 (2009).
[38]A. Amsden, P. O'Rourke, and T. Butler, "Kiva-II: A computer program for chemically reactive flows with sprays," Technical Report No. LA-11560-MS, Los Alamos National Lab, NM, 1989.
[39]S. O. Unverdi, "Numerical simulations of multi-fluid flows," Ph.D. thesis, The University of Michigan, 1990.
[40]S. O. Unverdi and G. Tryggvason, "A front-tracking method for viscous, incompressible, multi-fluid flows," J. Comput. Phys. **100**, 25 (1992).
[41]M. Nobari, Y. J. Jan, and G. Tryggvason, "Head-on collision of drops–A numerical investigation," Phys. Fluids **8**, 29 (1996).
[42]H. Lamb, *Hydrodynamics* (Cambridge University Press, 1932).
[43]E. Steinthorsson and G. Tryggvason, "A front tracking scheme for high density-ratio multi-fluid flows," AIAA Paper No. 99-3326, 1999.
[44]S. Thomas, A. Esmaeeli, and G. Tryggvason, "Multiscale computations of thin films in multiphase flows," Int. J. Multiphase Flow **36**, 71 (2010).
[45]H. Terashima and G. Tryggvason, "A front-tracking/ghost-fluid method for fluid interfaces in compressible flows," J. Comput. Phys. **228**, 4012 (2009).
[46]F. M. White and I. Corfield, *Viscous Fluid Flow* (McGraw-Hill, New York, 2006).